INTERNATIONAL JOURNAL FOR NUMERICAL METHODS IN ENGINEERING
Int. J. Numer. Meth. Engng 2006; **65**:1688–1713
Published online 6 October 2005 in Wiley InterScience (www.interscience.wiley.com). DOI: 10.1002/nme.1514

A mathematical framework of the bridging scale method

Shaoqiang Tang[1,2,*,†], Thomas Y. Hou[2,‡] and Wing Kam Liu[3,§]

[1]*LTCS, Department of Mechanics and Engineering Science, Peking University, Beijing 100871, People's Republic of China*
[2]*Applied and Computational Mathematics, Caltech, Pasadena, CA 91125, U.S.A.*
[3]*Department of Mechanical Engineering, Northwestern University, Evanston, IL 60208, U.S.A.*

SUMMARY

In this paper, we present a mathematical framework of the bridging scale method (BSM), recently proposed by Liu *et al*. Under certain conditions, it had been designed for accurately and efficiently simulating complex dynamics with different spatial scales. From a clear and consistent derivation, we identify two error sources in this method. First, we use a linear finite element interpolation, and derive the coarse grid equations directly from Newton's second law. Numerical error in this length scale exists mainly due to inadequate approximation for the effects of the fine scale fluctuations. An modified linear element (MLE) scheme is developed to improve the accuracy. Secondly, we derive an exact multiscale interfacial condition to treat the interfaces between the molecular dynamics region Ω_D and the complementary domain Ω_C, using a time history kernel technique. The interfacial condition proposed in the original BSM may be regarded as a leading order approximation to the exact one (with respect to the coarsening ratio). This approximation is responsible for minor reflections across the interfaces, with a dependency on the choice of Ω_D. We further illustrate the framework and analysis with linear and non-linear lattices in one-dimensional space. Copyright © 2005 John Wiley & Sons, Ltd.

KEY WORDS: multiscale computation; bridging scale method; coarse–fine decomposition; molecular dynamics coupled with finite elements

*Correspondence to: Shaoqiang Tang, Department of Mechanics and Engineering Science, Peking University, Beijing 100871, People's Republic of China.
† E-mail: maotang@pku.edu.cn
‡ E-mail: hou@acm.caltech.edu
§ E-mail: w-liu@northwestern.edu

Contract/grant sponsor: NSF; contract/grant numbers: FRG DMS-0353838, ITR ACI-0204932, IGERT
Contract/grant sponsor: Chinese Special Funds for Major State Basic Research Project; contract/grant number: G2000077305
Contract/grant sponsor: NSFC; contract/grant numbers: 90407021, 10271003

Received 18 February 2005
Revised 11 August 2005
Accepted 17 August 2005

1. INTRODUCTION

Along with the rapid progress in materials science and technology, there is an increasing demand for probing into fine space and time scales. With limited computing capabilities, the demand is partially fulfilled by describing a complex system with multiple scales. The crack problem, as an example, involves microscopic dynamics around the crack, as well as macroscopic behaviour for the bulk material. While the local dynamics evolve according to Newton's second law for atoms, the solid body can be approximated by linear elasticity far away from the crack. A multiscale method aims at incorporating models and numerical methods for these scales in a proper manner. A seamless treatment, namely, making them compatible, tries to avoid mismatch across scales.

During the last two decades, numerous multiscale methods have been developed and applied successfully in various applications for systems of atoms. Typically one performs molecular dynamics (MD) computation only in the localized region with active non-linear atomistic interactions, while a coarse grid description is used in the surrounding region. It is well known that the abrupt termination of the atomistic region leads to strong spurious wave reflection at the interface between the two scales [1]. Due to the interaction between regions, this reflection spreads error through the whole domain. Much research has been done in handling such reflection. Because the atomistic displacement includes various wave numbers, the governing equations of motion lead to dispersion during wave propagation. Therefore, interfacial conditions derived for scattering problems like non-reflecting boundary conditions and Dirichlet-to-Neumann methods cannot be applied here [2–5].

Most multiscale methods reduce interfacial reflection by making use of a handshaking region, such as in the finite elements and atomistic method [6], the coupling of length scales method, the coarse-grained molecular dynamics (CGMD) method, the macroscopic, atomistic, *ab initio* dynamics (MAAD) method, or the bridging domain method [7–10]. In this region, a certain weighted average is performed between the MD description and the coarse grid description. The perfectly matched layer (PML) method introduces a damping term to absorb reflections [11, 12]. Quite differently, the quasicontinuum (QC) method reduces the reflection with a gradually changing mesh, and uses representative atoms and the Cauchy–Born rule to compute strain energy in a solid body [13–15]. However, it applies mainly to static and quasi-static problems. The coupled atomistic and discrete dislocation (CADD) method [16, 17] has the same limitation.

Yet another interfacial treatment assumes linearity along a semi-infinite periodic chain. Based on the study of a harmonic lattice [18], the exact displacement of the first atom outside of the main MD region may be expressed as a convolution of the time history at the interfacial atom [19]. The bridging scale method (BSM) was introduced recently by Liu *et al*. through a series of papers, using this time history treatment essentially only for the fine fluctuation components in the displacement. See References [1, 20–22] and references therein.

In contrast to enormous efforts in designing multiscale algorithms, most existing methods are based on heuristic derivations or physical arguments. On the other hand, clear mathematical formulations and careful analysis are desired for applications and further improvements [23, 24]. In this paper, we shall present such an attempt in formulating and analysing BSM. Besides simplifying considerably the original derivations in Reference [1], we further identify two error sources in this method. First, numerical error in the coarse scale comes mainly from an linear element (LE) scheme, in which the effects of the fine scale fluctuations are inadequately accounted for. We further develop an modified linear element (MLE) scheme to improve the

accuracy. Secondly, in the original BSM formulation, a supplementary variable q was introduced, and the MD computation was performed in a mixture of the coarse scale description for u and the fine fluctuation in q. This causes inconsistency and complexity in deriving interfacial conditions. Under the coarse–fine decomposition with the linear element interpolation, and an assumption that the internal forces depend linearly on the fine fluctuations away from the MD region, an *exact* multiscale interfacial condition is derived for the first time in this paper. The interfacial condition used in the BSM implementations is actually a leading order approximation of the exact condition (with respect to the coarsening ratio). It is this approximation that is responsible for an energy interchange between the fine fluctuation and the mean displacement across the interfaces, and minor reflections with a dependency on the choice of Ω_D.

The major difference in the current paper from Reference [1] *lies in the consistent and rigorous derivation of governing equations for* u' *and* d, *and the exact multiscale interfacial conditions. These equations enable us to analyse error sources in BSM.*

The rest of this paper is organized as follows. We shall formulate BSM in Section 2, particularly the coarse grid equations and interfacial conditions. In Section 3, we apply it to harmonic and anharmonic lattices in one-dimensional space, as well as a lattice with a Lennard–Jones potential. Some concluding remarks are made in the last section.

2. GENERAL FORMULATION

Consider a material system in $\Omega \subset \mathbb{R}^3$, consisting of n_a atoms. The position of the nth atom at rest is x_n. Under suitable initial and boundary conditions, the motion of each atom is governed by Newton's second law

$$M_A \ddot{u} = f + f_{\text{ext}} \tag{1}$$

with $u, f, f_{\text{ext}} \in \mathbb{R}^{3n_a}$ representing the displacement, internal force and external force, respectively. The mass matrix is $M_A = \text{diag}(m_1 I_{3\times 3}, \ldots, m_{n_a} I_{3\times 3})$ where $m_i > 0$. The internal force comes from interactions among atoms, described by a potential U. When a rest frame is used, the potential is a function of atom displacements, and

$$f = -\nabla_u U(u) \tag{2}$$

BSM contains the following ingredients:

- We define a coarse grid over the whole domain Ω. At each coarse grid point y_J $(J = 1, \ldots, n_c)$, we assign a displacement d_J. They form a coarse grid displacement vector d.
- By the projections to be defined later on, we decompose the displacement u into a mean displacement $\bar{u}$, and a fine fluctuation u'. In particular, the mean displacement has a relatively longer characteristic length, and may be expressed by a linear interpolation of the coarse grid displacement d.
- Assuming that strong coupling between $\bar{u}$ and u' occurs in a certain localized subdomain Ω_D only. We perform MD computations solely in Ω_D, and separate the physical domain Ω into two subdomains, namely Ω_D and $\Omega_C = \Omega \backslash \Omega_D$.

In the following, we shall extensively use subscript D to denote quantities in Ω_D, and C for those in Ω_C. For instance, the displacement vector is taken as $u = \begin{bmatrix} u_D \\ u_C \end{bmatrix}$.

We perform macroscopic (MC) computations for the evolution of d over the whole domain. In Ω_C, fine fluctuations in the atomistic motion are assumed to be negligible. We therefore describe the motion only in the coarse grid. On the other hand, detailed MD computations are performed in Ω_D, to accurately capture the non-linear dynamics. Compared with a full MD simulation, the computing load and memory requirement are greatly reduced.

We remark that most existing multiscale methods utilize a *handshaking* region, and make a certain average of the MD and MC description in this region [7–9]. A coupled system for MD and MC variables are formed and solved numerically. The averaged description in the handshaking region is empirical, and the related error is usually hard to control.

In contrast, we use an *overlapping* region. That is, we compute both d and u in Ω_D. In general, these two quantities are not guaranteed to evolve in a consistent way. We regard the MD solution u_D as a more accurate description, and modify accordingly the coarse grid displacement d. This is explained in more detail in Section 2.1. The use of the overlapping region allows us to compute separately the MD solution and MC solution with different time-step sizes. The algorithm is clearer, and easier to implement.

We note that in Reference [1], the governing equations of $\bar{u}$ and u' involve the supplementary displacement q. In particular, MD computations for q_D are performed in Ω_D. Displacement was obtained through $u_D = \bar{u}_D + q'_D$. As we shall further explain in Section 2.2, this causes inconsistency in posing the interfacial conditions. In contrast, here we derive the precise governing equations for u', without the redundant supplementary displacement q. MD computations are performed for u_D. This makes the framework compact, and allows us to derive a multiscale interfacial condition, which is exact for linear lattices.

Throughout this paper, we shall confine ourselves to situations where only a linear effect of the fine fluctuation u'_C on mean motion is accounted for in Ω_C. This assumption fails for lattice systems with finite temperature. We remark that some progresses have been made recently for treating non-zero temperature within the BSM framework [20].

In the presentation of BSM, we describe the following main issues in Sections 2.1 and 2.2. We give a flowchart of the algorithm in Section 2.3.

- We decompose the displacement u into $\bar{u}$ and u'. We relate $\bar{u}$ and d by an interpolation matrix, corresponding to the linear finite element.
- We derive the governing equation for the dynamics of d. Because d is defined at coarse grid points over the whole domain Ω, boundary conditions are naturally obtained from the physical problem setting.
- We specify the interfacial condition for MD computation on Ω_D. While the equations are just Newton's second law, we need to specify boundary conditions. The boundary of Ω_D may consist of physical boundaries and Ω_C/Ω_D interfaces. The dynamics of an atom at a physical boundary is prescribed by the problem setting. In contrast, internal force on an interfacial atom may involve nearby atoms in Ω_C (ghost points), for which we do not have detailed description about the fine fluctuation. We reconstruct u' at ghost point atoms by using the time history kernel technique, described in Section 2.2.

2.1. Displacement decomposition and coarse grid equation

A linear finite element is adopted for interpolation. That is, we take a linear shape function matrix N of size $3n_a \times 3n_c$, and each component of d stands for displacement at a finite element nodal point. We recall that n_a and n_c are the number of the atoms, and the number

of the coarse grid points, respectively. To get the optimal approximation of u, we minimize the residual $(u - Nd)^{\mathrm{T}} M_A (u - Nd)$. It is solved by

$$d = M^{-1} N^{\mathrm{T}} M_A u \tag{3}$$

Here, the effective mass matrix $M = N^{\mathrm{T}} M_A N$ is symmetric, positive definite, and $\mathrm{rank}(M) = 3n_c$. We call the displacement approximation $\bar{u} = Nd$ the mean displacement, and the deviation $u' = u - \bar{u}$ the fine fluctuation. This defines a coarse–fine decomposition

$$\bar{u} = Pu = Nd, \quad u' = Qu \tag{4}$$

with projection operators $P = NM^{-1}N^{\mathrm{T}}M_A$ and $Q = I - P$.

The dynamics of the coarse grid variable d is obtained when we multiply (1) from the left by $M^{-1}N^{\mathrm{T}}$

$$\ddot{d} = M^{-1} N^{\mathrm{T}} (f + f_{\mathrm{ext}}) \tag{5}$$

From $U(u) = U(Nd + u')$ and the chain rule, we may rewrite it as

$$M\ddot{d} = -\nabla_d U(Nd + u') + N^{\mathrm{T}} f_{\mathrm{ext}} \tag{6}$$

This resembles Newton's second law over the coarse grid, if we view M as 'mass', and d as displacement at coarse grid points.

Equation (6) is valid in the whole domain Ω. With the presence of fine fluctuation u', no approximation has been made so far. However, in a multiscale method, we avoid computing the fine fluctuations u'_C. To get a governing equation in closed form, we should make approximations to incorporate the effect of u'_C properly.

We propose to simulate the dynamics of d in the following way. For each coarse scale time step, we first compute an intermediate value $\tilde{d}$ with a coarse grid equation in closed form. In the numerical examples to be presented later in this paper, we basically drop out u' terms to get an linear element (LE) scheme. That is, with profile $(\tilde{d}(t^n), \dot{\tilde{d}}(t^n)) = (d(t^n), \dot{d}(t^n))$, we use

$$M\ddot{\tilde{d}} = -\nabla_{\tilde{d}} U(N\tilde{d}) + N^{\mathrm{T}} f_{\mathrm{ext}} \tag{7}$$

to get $(\tilde{d}(t^{n+1}), \dot{\tilde{d}}(t^{n+1}))$.

In general, this may not adequately resolve the mean displacement in Ω_D, where complicated non-linear dynamics occur. By construction, the non-linear dynamics are resolved by the MD computation of u_D. Therefore, we combine the information of $(\tilde{d}(t^{n+1}), \dot{\tilde{d}}(t^{n+1}))$ and $(u_D(t^{n+1}), \dot{u}_D(t^{n+1}))$ to get d and $\dot{d}$. More precisely, we approximate $u_C(t^{n+1})$ by $\bar{u}_C(t^{n+1}) = N_C \tilde{d}(t^{n+1})$. This gives

$$u(t^{n+1}) \approx \begin{bmatrix} u_D(t^{n+1}) \\ \\ N_C \tilde{d}(t^{n+1}) \end{bmatrix} \tag{8}$$

This amounts to

$$d(t^{n+1}) = M^{-1} N^{\mathrm{T}} M_A u(t^{n+1}) \approx \tilde{d}(t^{n+1}) + M^{-1} \begin{bmatrix} N_D^{\mathrm{T}} M_{A_D} u_D(t^{n+1}) - N_D^{\mathrm{T}} M_{A_D} N_D \tilde{d}(t^{n+1}) \\ 0 \end{bmatrix} \tag{9}$$

Recall that corresponding to the domain decomposition, we take

$$N = \begin{bmatrix} N_D \\ \\ N_C \end{bmatrix}, \quad M_A = \begin{bmatrix} M_{A_D} & \\ & M_{A_C} \end{bmatrix} \tag{10}$$

The velocity $\dot{d}(t^{n+1})$ is obtained in a similar way.

Instead of (7) and (9), there are more sophisticated ways to design schemes for d. For instance, we propose an MLE scheme for a harmonic lattice in Section 3.1.2. It resolves the mean displacement better than (7) in Ω_C. As we shall illustrate later, a more accurate coarse grid scheme has a limited effect in reducing the reflections. For many applications, designing an accurate interfacial condition is the main issue.

Now we make a few remarks. First, the effects of the MD solution u_D should be accounted for the coarse scale dynamics in a proper manner. Many existing multiscale methods couple them through certain hybrid descriptions such as a mixed Hamiltonian in a handshaking region. Our approach avoids such a mixed description. The error in this step is just due to neglecting u'_C in the projection, which is small by construction and well under control. Secondly, we use only Newton's second law for u to derive the coarse grid equations. In the literature, other approaches have been proposed to get equations in closed form. For instance, with the Cauchy–Born rule, the stress is obtained by considering locally uniform strain. This has been adopted in both the quasi-continuum method [15] and the original version of BSM [1]. Meanwhile, Qian *et al.* proposed a virtual atom cluster (VAC) method under the BSM framework [25]. We sketch its basic idea in the Appendix A. Thirdly, we will introduce a time history treatment to get an expression of u'_C in Section 2.2. With some additional computing load, it is then possible to further elaborate on the coarse grid equation. Finally, we remark that a systematic way for deriving accurate and efficient coarse grid equations has been proposed in Reference [26].

2.2. *Interfacial conditions and time history kernel*

It is well-known that a special treatment is required in posing conditions for Ω_C/Ω_D interfacial atoms, to avoid a non-physical reflection. We adopt a time history kernel technique proposed for a harmonic lattice by Adelmann and Doll [18]. Briefly speaking, after making a linearization, we reconstruct u' at ghost point atoms from the time history of fine fluctuations at related interfacial atoms. The mean displacement is readily obtained by interpolating d. The summation of these two parts provides the displacement at ghost point atoms, serving as the interfacial conditions for MD computations in Ω_D.

Noticing the symmetry of M and M_A, we derive for the projection $Q = I - P$

$$Q^{\mathrm{T}} M_A = M_A - M_A N M^{-1} N^{\mathrm{T}} M_A = M_A Q \tag{11}$$

Multiplying Q^{T} to (1) and noticing the definition $u' = Qu$, we obtain the governing equation for u'

$$M_A \ddot{u}' = Q^{\mathrm{T}}(f + f_{\mathrm{ext}}) \tag{12}$$

Next, we make a linearization of the internal force under the assumption that u'_C is small

$$f(u) \approx \tilde{f}(\bar{u}, u'_D) + K(\bar{u}, u'_D)u'_C$$
$$K(\bar{u}, u'_D) = \begin{bmatrix} K_D \\ K_C \end{bmatrix} = \begin{bmatrix} \nabla_{u_C} f_D(\bar{u}, u'_D) \\ \nabla_{u_C} f_C(\bar{u}, u'_D) \end{bmatrix} \tag{13}$$

Here K is a submatrix of the stiffness matrix $\nabla_u f(u)$. In fact, the ghost point atoms (in Ω_C) and the interfacial atoms (in Ω_D) are determined from non-zero entries of K_D. If the ith row in K_D contains a non-zero entry, the corresponding u_i (an entry in u_C) exerts an internal force on certain atom(s) in Ω_D. The ith atom in Ω_C is a ghost point, and the corresponding atoms in Ω_D receiving internal force are interfacial atoms.

From its general form, $K = K(\bar{u}, u'_D)$ depends on both the mean displacement $\bar{u}$ and the fine fluctuation u'_D. Hence it is time dependent, and the time history treatment to be described below fails in general. In many applications, however, we may take K for a lattice at rest to approximate $K(\bar{u}, u'_D)$. In the following discussions we shall use such a time-independent K.

Collecting forces independent of u'_C in

$$f^*(\bar{u}, u'_D) = \tilde{f}(\bar{u}, u'_D) + f_{\text{ext}} \tag{14}$$

we end up with an approximate linear equation

$$M_{A_C}\ddot{u}'_C = Q_C^{\mathrm{T}}(f^*(\bar{u}, u'_D) + Ku'_C) \tag{15}$$

Because M_{A_C}, Q_C and K are time independent matrices, we apply a Laplace transform (denoted by $\hat{\ }$) to (15)

$$M_{A_C}[s^2\widehat{u'_C} - su'_C(0) - \dot{u}'_C(0)] = Q_C^{\mathrm{T}}[\widehat{f^*}(\bar{u}, u'_D) + K\widehat{u'_C}] \tag{16}$$

The solution is

$$\widehat{u'_C} = (s^2 I - M_{A_C}^{-1} Q_C^{\mathrm{T}} K)^{-1}[M_{A_C}^{-1} Q_C^{\mathrm{T}} \widehat{f^*}(\bar{u}, u'_D) + su'_C(0) + \dot{u}'_C(0)] \tag{17}$$

We only need a few components in u'_C that correspond to the ghost point atoms for the MD computations. The inverse Laplace transform is taken for these components. For each ghost point atom, we take a corresponding row from the time history kernel matrix

$$\Phi = \mathscr{L}^{-1}[(s^2 I - M_{A_C}^{-1} Q_C^{\mathrm{T}} K)^{-1}] \tag{18}$$

Let the submatrix formed by these rows be $\Phi_G(t)$. The fine fluctuation at the ghost point atoms is

$$u'_G = \Phi_G(t) * [M_{A_C}^{-1} Q_C^{\mathrm{T}} f^*(\bar{u}, u'_D)] + \dot{\Phi}_G(t)u'_C(0) + \Phi_G(t)\dot{u}'_C(0) \tag{19}$$

This provides conditions for the interfacial atoms. *Under the assumptions mentioned above, i.e. the localized fine fluctuation and the constant approximation of* K, (18) *and* (19) *form an exact multiscale interfacial condition for the BSM formulation*. However, M^{-1} is typically a full matrix, and so are Q and Q_C. Even for a simple K, the kernel Φ is a full matrix, and the inverse transform may not be easy to compute. Therefore, it demands heavy computing load and memory to implement the exact multiscale interfacial condition (18) with (19). On

the other hand, in the limit of an infinite coarsening ratio, it may be shown that all entries in M^{-1} and P tend to zero. Accordingly, we approximate Q by the identity matrix I, and the interfacial condition (19) by

$$u'_G \approx \Theta_G(t) * [M_{A_C}^{-1} f_C^*(\bar{u}, u'_D)] + \dot{\Theta}_G(t) u'_C(0) + \Theta_G(t) \dot{u}'_C(0) \tag{20}$$

with

$$\Theta = \mathscr{L}^{-1}[(s^2 I - M_{A_C}^{-1} K_{CC})^{-1}] \tag{21}$$

Here K_{CC} is the lower-right block of K corresponding to Ω_C. With this simplification, we notice that only a sub-vector of $f^*(\bar{u}, u'_D)$ needs to be memorized and convoluted. We note that the complicated derivation presented in Reference [1] actually amounts to this approximation. Furthermore, if the lattice has a repeated structure, we may compute the time history kernel with the help of Fourier and Laplace transforms [1, 27, 28].

A few remarks are as follows. First, *the simplification made in BSM causes numerical error across the interfaces. However, when the linear element interpolation N is adopted for coarse–fine decomposition, we have to make this simplification to avoid complete evaluation of the full matrix convolution in* (19). Secondly, the initial data $(u'_C(0), \dot{u}'_C(0))$ are rarely available in Ω_C for real applications. They are either ignored, or substituted by random fields. In particular, suitable random fields may approximate a heat bath of finite temperature [20]. Thirdly, if no coarse–fine decomposition is performed for the displacement, the exact interfacial condition reads $u_G = \Theta_G(t) * [M_{A_C}^{-1} f_C^*] + \dot{\Theta}_G(t) u_C(0) + \Theta_G(t) \dot{u}_C(0)$ [19]. On the other hand, the coarse–fine decomposition allows us to deal with applications when there are both incoming and outgoing long waves, which are treated by the coarse grid computations. Finally, we may perform displacement decomposition in a better way to avoid interactions between $\bar{u}$ and u' [26]. The reflection is further reduced, because the convolution is performed only with u', which typically represents a small part of the total energy.

We further mention that if the coarse grid equations are given for the continuum (e.g. Navier–Stokes equations), special interfacial treatments have been developed, such as a hybrid method (for fluids) in References [29, 30], and a dynamic atomistic-continuum method in Reference [31].

2.3. Numerical scheme

We describe a verlet algorithm for time integration of a dynamical system

$$\ddot{q} = A(q, t) \tag{22}$$

With a time step size $\triangle t$ and data $q(t^n) = q^n, \dot{q}(t^n) = \dot{q}^n$, we first compute the acceleration $A^n = A(q^n, t^n)$. This is used for updating one step for q and half step for $\dot{q}$ by

$$q^{n+1} = q^n + \dot{q}^n \triangle t + A^n \frac{(\triangle t)^2}{2}, \quad \dot{q}^{n+1/2} = \dot{q}^n + A^n \frac{\triangle t}{2} \tag{23}$$

Then we compute the new acceleration $A^{n+1} = A(q^{n+1}, t^{n+1})$, and update another half step for $\dot{q}$ by

$$\dot{q}^{n+1} = \dot{q}^{n+1/2} + A^{n+1} \frac{\triangle t}{2} \tag{24}$$

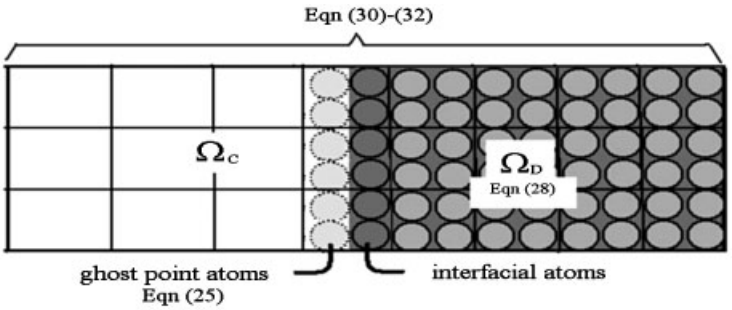

Figure 1. Illustration of the computing mesh for BSM.

This is applied for both the dynamics of d in the coarse grid, and Newton's second law for u_D in Ω_D. Furthermore, we use a mixed time integration technique in BSM, i.e. we use a small time step size $\triangle\tau$ in MD computation of u_D, and $\triangle t = m\triangle\tau$ in the MC computation of d.

We summarize the BSM (Figure 1) scheme in the following list, for updating one big time step $\triangle t$:

1. MD computation in Ω_D.
   - Holding the velocity and acceleration of d fixed at t^n, we obtain the mean displacement $\bar{u}$ at the interfacial atoms and the ghost point atoms at sub-time steps $t^n + k\triangle\tau$ (for $k = 1, \ldots, m$).
   - At a sub-time step, we compute the fine fluctuation at the ghost point atoms u'_G with time step size $\triangle\tau$ from (Equations (20) and (21) in Section 2.2)

$$u'_G \approx \Theta_G(t) * [M_{A_C}^{-1} f_C^*(\bar{u}, u'_D)] + \dot{\Theta}_G(t) u'_C(0) + \Theta_G(t) \dot{u}'_C(0) \tag{25}$$

   Here f^* collects all forces independent of u'_C

$$f_C^*(\bar{u}, u'_D) = \tilde{f}_C(\bar{u}, u'_D) + f_{\text{ext},C} \tag{26}$$

   and $\Theta_G(t)$ is a sub-matrix of

$$\Theta = \mathscr{L}^{-1}[(s^2 I - M_{A_C}^{-1} K_{CC})^{-1}] \tag{27}$$

   In Ω_D, we compute a subsystem of Newton's second law

$$M_{A_D} \ddot{u}_D = f_D + f_{\text{ext},D} \tag{28}$$

   with the interfacial conditions of ghost point atom displacement

$$u_G = \bar{u}_G + u'_G \tag{29}$$

   We update the time history of $M_{A_C}^{-1} f_C^*(\bar{u}, u'_D)$ after each sub-time step.

2. Coarse grid computation in Ω.
   - We compute $(\tilde{d}^{n+1}, \dot{\tilde{d}}^{n+1})$ with $(\tilde{d}^n, \dot{\tilde{d}}^n) = (d^n, \dot{d}^n)$ from (Equation (7) in Section 2.1)

$$M\ddot{\tilde{d}} = -\nabla_{\tilde{d}} U(N\tilde{d}) + N^{\mathrm{T}} f_{\mathrm{ext}} \tag{30}$$

     We remark that one may use other methods such as an MLE scheme, to be described, or the VAC method (A2) in Appendix A.
   - Making use of the MD solution at $t^n + m\triangle\tau = t^n + \triangle t$, we assign (Equation (9) in Section 2.1)

$$d^{n+1} = \tilde{d}^{n+1} + M^{-1} \begin{bmatrix} N_D^{\mathrm{T}} M_{A_D} u_D^{n+1} - N_D^{\mathrm{T}} M_{A_D} N_D \tilde{d}^{n+1} \\ 0 \end{bmatrix} \tag{31}$$

     and

$$\dot{d}^{n+1} = \dot{\tilde{d}}^{n+1} + M^{-1} \begin{bmatrix} N_D^{\mathrm{T}} M_{A_D} \dot{u}_D^{n+1} - N_D^{\mathrm{T}} M_{A_D} N_D \dot{\tilde{d}}^{n+1} \\ 0 \end{bmatrix} \tag{32}$$

As the reassignment (31) and (32) are always performed, in the following discussions we shall simply write $\tilde{d}$ in the coarse grid equation (30) as d, without making any ambiguity.

3. APPLICATIONS

3.1. Harmonic lattice

A harmonic lattice is the simplest model for molecular dynamics of a crystal, and serves as a test problem for multiscale methods. The exact solution is available due to linearity. A precise quantitative analysis can be used to make an error estimate and study the accuracy of the method.

3.1.1. Problem setting. Consider a harmonic lattice in one-dimensional space with n_a atoms. The position of the nth atom at rest is $x_n = -L + nh_a$ for $n = 1, \ldots, n_a$, with $2L = (n_a + 1)h_a$, as shown in Figure 2. Its displacement is denoted by $u_n(t)$. With both ends fixed, we consider a nearest neighbour interaction. We scale time by $\sqrt{m_a/k}$, with m_a the mass and k the spring

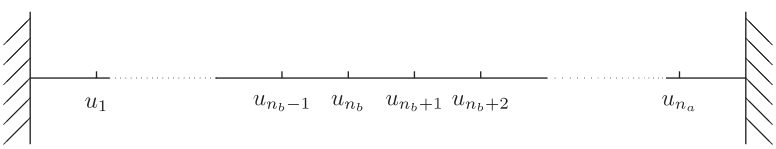

Figure 2. Harmonic lattice in one-dimensional space.

constant. The rescaled governing equations are

$$\ddot{u} = D_A u, \quad D_A = \begin{bmatrix} -2 & 1 & & \\ 1 & -2 & \ddots & \\ & \ddots & \ddots & 1 \\ & & 1 & -2 \end{bmatrix}_{n_a \times n_a} \tag{33}$$

A coarse grid point is placed every p atoms, at $y_J = -L + Jh_e$ for $J = 1, \ldots, n_c$, where $h_e = ph_a$ and $n_a + 1 = p(n_c + 1)$.

In numerical simulations, we shall always take $h_a = 0.005$, $p = 10$, $h_e = ph_a = 0.05$. The initial data is set by $u_n(0) = u^0(x_n)$ with

$$u^0(x) = \begin{cases} 0.005 \dfrac{e^{-100x^2} - e^{-6.25}}{1 - e^{-6.25}} (1 + 0.1\cos(80\pi x)), & |x| \leqslant 0.25 \\ 0 & \text{elsewhere} \end{cases} \tag{34}$$

3.1.2. Coarse grid equations. Let $a = \frac{1}{p}[p-1, \cdots, 1, 0]^{\mathrm{T}}$, and $b = \frac{1}{p}[1, \cdots, p]^{\mathrm{T}}$. The shape function matrix is

$$N = \begin{bmatrix} 1 & & & & \\ a & b & & & \\ & \ddots & \ddots & & \\ & & & a & b \end{bmatrix} \tag{35}$$

This corresponds to a linear interpolation $\bar{u}_{Ip+k} = ((p-k)d_I + kd_{I+1})/p$.

From (33), we observe that each atom has a unitary mass after rescaling. This gives a mass matrix $M_A = I$. The effective mass matrix is then

$$M = N^{\mathrm{T}} N = \begin{bmatrix} \alpha_0 & \beta & & & \\ \beta & \alpha & \beta & & \\ & \ddots & \ddots & \ddots & \\ & & \beta & \alpha & \beta \\ & & & \beta & \alpha_0 \end{bmatrix} \tag{36}$$

with $\alpha_0 = 1 + a^{\mathrm{T}}a = b^{\mathrm{T}}b = (p+1)(2p+1)/6p$, $\alpha = a^{\mathrm{T}}a + b^{\mathrm{T}}b = (2p^2+1)/3p$, $\beta = a^{\mathrm{T}}b = (p^2-1)/6p$.

Now (6) reads

$$(M\ddot{d})_J = \frac{1}{p}(d_{J-1} - 2d_J + d_{J+1} + u'_{(J-1)p} - 2u'_{Jp} + u'_{(J+1)p}) \tag{37}$$

We call it an linear element with molecular dynamics information (LEMD) scheme. Dropping the u' terms, we obtain an LE scheme, corresponding to (30)

$$(M\ddot{d})_J = \tfrac{1}{p}(d_{J-1} - 2d_J + d_{J+1}) \tag{38}$$

A modified version may be derived as follows. Noticing that $u_{Jp} = d_J + u'_{Jp}$, we rewrite (37) as

$$(M\ddot{d})_J = \tfrac{1}{p}(u_{(J-1)p} - 2u_{Jp} + u_{(J+1)p}) \tag{39}$$

Or in a vector form,

$$M\ddot{d} = \tfrac{1}{p}DV \tag{40}$$

Here D is in the same form as D_A but of size $n_c \times n_c$, and $V = [u_p, \ldots, u_{n_c p}]^{\mathrm{T}}$.

The second-order spatial derivative u_{xx} at $y_J = x_{Jp}$ may be approximated by either $(u_{Jp-1} - 2u_{Jp} + u_{Jp+1})/h_a^2$ in the fine grid, or $(d_{J-1} - 2d_J + d_{J+1})/(ph_a)^2$ in the coarse grid. Accordingly, we approximate Newton's second law for the (Jp)th atom by

$$\ddot{u}_{Jp} = u_{Jp-1} - 2u_{Jp} + u_{Jp+1} \approx (d_{J-1} - 2d_J + d_{J+1})/p^2 \tag{41}$$

In a vector form, this gives

$$\ddot{V} \approx Dd/p^2 \tag{42}$$

Now, we differentiate (40) twice with respect to time to get

$$M\frac{\mathrm{d}^4}{\mathrm{d}t^4}d = \frac{1}{p^3}D^2 d \tag{43}$$

It may be shown that away from the boundary, M and D share the same set of eigenvectors, and $\sqrt{M}D = D\sqrt{M}$. This allows us to decompose (43) into

$$\left(\sqrt{M}\frac{\mathrm{d}^2}{\mathrm{d}t^2} + \frac{1}{\sqrt{p^3}}D\right)\left(\sqrt{M}\frac{\mathrm{d}^2}{\mathrm{d}t^2} - \frac{1}{\sqrt{p^3}}D\right)d = 0 \tag{44}$$

The first operator is unstable, therefore irrelevant to the physical problem. An MLE scheme then follows:

$$\sqrt{M}\ddot{d} = \frac{1}{\sqrt{p^3}}Dd \tag{45}$$

We shall refer to the multiscale method using the LE scheme for coarse grid computation as the BSM-LE scheme, and that using the MLE scheme as the BSM-MLE scheme.

3.1.3. Interfacial conditions. We now turn to ghost point atom displacement. To make it precise, we consider an Ω_C/Ω_D interface at the n_bth atom, as shown in Figure 2. It is recognized that

M_{A_C} is an identity matrix, $K_C = D_C$. Corresponding to (26), we have

$$f^* = \begin{bmatrix} D_D u_D + (0, \ldots, 0, \bar{u}_{n_b+1})^{\mathrm{T}} \\ D_C \bar{u}_C + (u'_{n_b}, 0, \ldots, 0)^{\mathrm{T}} \end{bmatrix}, \quad K_D = \begin{bmatrix} 0 & 0 & \cdots & 0 \\ \vdots & \vdots & & \vdots \\ 0 & 0 & \ldots & 0 \\ 1 & 0 & \cdots & 0 \end{bmatrix} \tag{46}$$

After some manipulations, we find (19) as

$$\begin{aligned} u'_{n_b+1} = \phi_1 * u'_{n_b} + \Phi_G * [I_C(D_A P - P D_A)\bar{u} - P_{CD} D_D u'_D \\ - P_{CC}(u'_{n_b}, 0, \ldots, 0)^{\mathrm{T}}] + \dot{\Phi}_G u'_C(0) + \Phi_G \dot{u}'_C(0) \end{aligned} \tag{47}$$

where $\Phi_G = [\phi_1, \ldots, \phi_{n_a - n_b}]$, $I_C = [0_{n_b \times n_b}, I_{(n_a - n_b) \times (n_a - n_b)}]$, and $P_C = [P_{CD}, P_{CC}]$ is a submatrix of $P = N M^{-1} N^{\mathrm{T}}$. Making use of the form of K_D, as shown in (18), Φ_G is the first row of

$$\mathscr{L}^{-1}\left[(s^2 I - Q_C^{\mathrm{T}} K)^{-1}\right] = \mathscr{L}^{-1}[(s^2 I - D_C + P_{CC} D_C + P_{CD} K_D)^{-1}] \tag{48}$$

Implementation of the *exact* interfacial condition (47) causes heavy computing load. From (36), we notice that diagonal entries of order p dominate the effective mass matrix M. This corresponds to a 'lumped mass' at the coarse grid points. Then, each entry in $P = N M^{-1} N^{\mathrm{T}}$ is of the order $1/p$. When p is big enough, we neglect P in the previous expressions as a leading order approximation. The formulae (47) and (48) are approximated by

$$u'_{n_b+1} \approx \phi_1 * u'_{n_b} + \dot{\Theta}_G u'_C(0) + \Theta_G \dot{u}'_C(0) \tag{49}$$

$$\Phi = \mathscr{L}^{-1}((s^2 I - Q_C^{\mathrm{T}} K)^{-1}) \approx \Theta = \mathscr{L}^{-1}((s^2 I - D_C)^{-1}) \tag{50}$$

They correspond to (20) and (21), respectively. Direct computation shows that the (1,1) entry in $(s^2 I - D_C)^{-1}$ is

$$\hat{\theta} = S \frac{1 - S^{2*N}}{1 - S^{2*(N+1)}} \overset{N \to +\infty}{\longrightarrow} S \tag{51}$$

with $S = [s^2 + 2 - s\sqrt{s^2 + 4}]/2$. Therefore, we approximate

$$\phi_1(t) \approx \theta(t) \approx \mathscr{L}^{-1}(S) = -\left(\frac{J_1(2t)}{t}\right)' = \frac{2 J_2(2t)}{t} \tag{52}$$

If the initial fine fluctuation is ignored in Ω_C, we have

$$u_{n_b+1} \approx \overline{u}_{n_b+1} + \theta(t) * u'_{n_b}(t) \tag{53}$$

We note that when $t \to +\infty$, we have $J_n(t) \approx \sqrt{2/\pi t}\cos(t - n\pi/2 - \pi/4)$. In our numerical implementation, we only keep a partial history $u'_{n_b}(\tau)$ for $\tau \in [t - T, t]$. This introduces an additional numerical error

$$\left| \int_0^{t-T} \theta(t-\tau) g(\tau)\, \mathrm{d}\tau \right| \leqslant \|g\|_{L^2([0,t-T])} \|\theta\|_{L^2([T,t])} \leqslant C \|g\|_{L^2([0,\infty))} T^{-1} \tag{54}$$

Numerical experiments indicate that the time history cut-off is only a secondary error source, compared with those incurred in other approximations such as throwing away the P-related terms.

3.1.4. Numerical results. First, we compare different coarse grid schemes, by numerical tests in the domain $x \in [-2, 2]$ without the time history kernel. Solutions at time $t = 150$ are depicted in Figure 3. Because of the finite propagation speed, the lattice is essentially at equilibrium far away. Furthermore, the system has a symmetry $x \to -x$, which is preserved by our numerical schemes. Therefore, we only plot solutions in a part of the computational domain.

The exact solution is computed by a full MD simulation with $\triangle\tau = 0.005$. In Figure 3, we observe that the primary wave (solid line) moves to around $x = h_a * t = 0.75$, whereas the fine fluctuation propagates slower.

With $p = 10$, the coarse grid schemes are tested for $\triangle t = 0.05$. The fine fluctuations could not be reproduced in such a coarse grid. With the exact solution at hand, the LEMD scheme reproduces the mean of the solution faithfully.

The LE scheme produces a faster phase speed at the wave front, accompanied by a kink. In contrast, the MLE scheme resolves the mean displacement very well. These are clearly explained by their dispersion relations. In fact, for a monochromatic wave in the form of $u_n(t) = \mathrm{e}^{\mathrm{i}(\lambda t - \omega n)}$, we find $\lambda = 2\sin(\omega/2)$. Meanwhile, substituting this form into the LE scheme (38) and the MLE scheme (45), we obtain dispersion relations for these two schemes. Please refer to

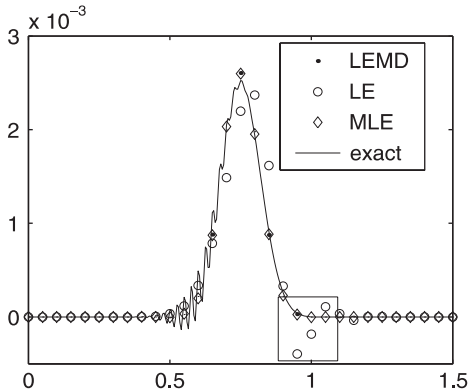

Figure 3. Harmonic lattice $u(x, 150)$: by LEMD, LE and MLE schemes. The LE scheme produces faster propagation speed, as highlighted in the boxed region.

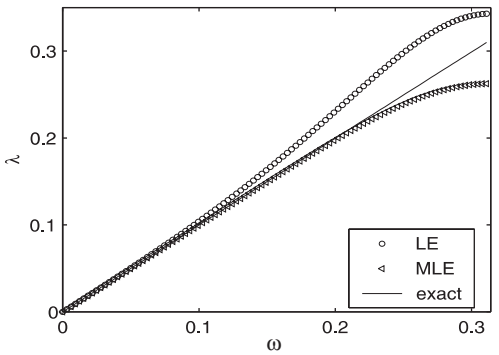

Figure 4. Dispersion relation for harmonic lattice by LE and MLE schemes: round frequency in time is plotted versus wave number $\omega \in [0, \pi/10]$.

Appendix B for more details

$$\lambda_{\mathrm{LE}} = \frac{2\sin(\omega p/2)}{\sqrt{p^2 - 2(p^2-1)\sin^2(\omega p/2)/3}}, \quad \lambda_{\mathrm{MLE}} = \frac{2\sin(\omega p/2)}{\sqrt[4]{p^4 - 2p^2(p^2-1)\sin^2(\omega p/2)/3}} \tag{55}$$

The dispersion relations are displayed in Figure 4. It is obvious that $\lambda_{\mathrm{LE}}(\omega) > \lambda(\omega)$.

Next, we compute by the BSM. The time history is kept for $T = 5$. We take $\Omega_D = [-0.375, 0.375]$, containing 151 atoms.

The solution at various times is shown in Figure 5, computed by the BSM-LE scheme. At time $t = 50$, oscillations have not reached the interface, and no reflection is observed. In a later stage, oscillations go across the interface, and minor reflection is observed. Reflection appears to vary slowly with a fairly long wavelength in space, in contrast to the short wavelength of fine fluctuation in the exact solution. At $t = 150$, oscillations have already passed the Ω_C/Ω_D interface. A small amount of energy is left in Ω_D. We also note that the LE scheme produces a small kink ahead of the wave front.

If we use the BSM-MLE scheme instead, the evolution remains similar. Better resolution is achieved in Ω_C, as shown in Figure 6. However, bigger reflections are observed. This sounds paradoxical, as the MLE scheme resolves the coarse grid solution better than the LE scheme. In fact, the major reason for interfacial reflection is the approximated interfacial condition, where the projection matrix P-related terms are dropped out. As we shall show in a moment, there is an energy interchange between the mean displacement and fine fluctuations. The truncation error due to the coarse grid scheme then becomes of secondary importance for accuracy. For instance, if we take an enlarged $\Omega_D = [-0.425, 0.425]$ instead (containing 161 atoms), the exact multiscale interfacial condition changes. However, after dropping out the P-related terms, we still use the same interfacial conditions (52) and (53). In subplots (a) and (b) of Figure 7, we clearly observe that reflections become comparable between the BSM-LE and the BSM-MLE schemes. Nevertheless, in all cases, the reflections have been considerably reduced, compared with the results by the LE scheme without time history kernel treatment, which are shown in subplots (c) and (d) of Figure 7.

We notice that reflections by the BSM method contain mainly long waves, in contrast with short wave reflection in subplots (c) and (d) of Figure 7. This indicates that the error does not come directly from the short wave absorption in the time history kernel

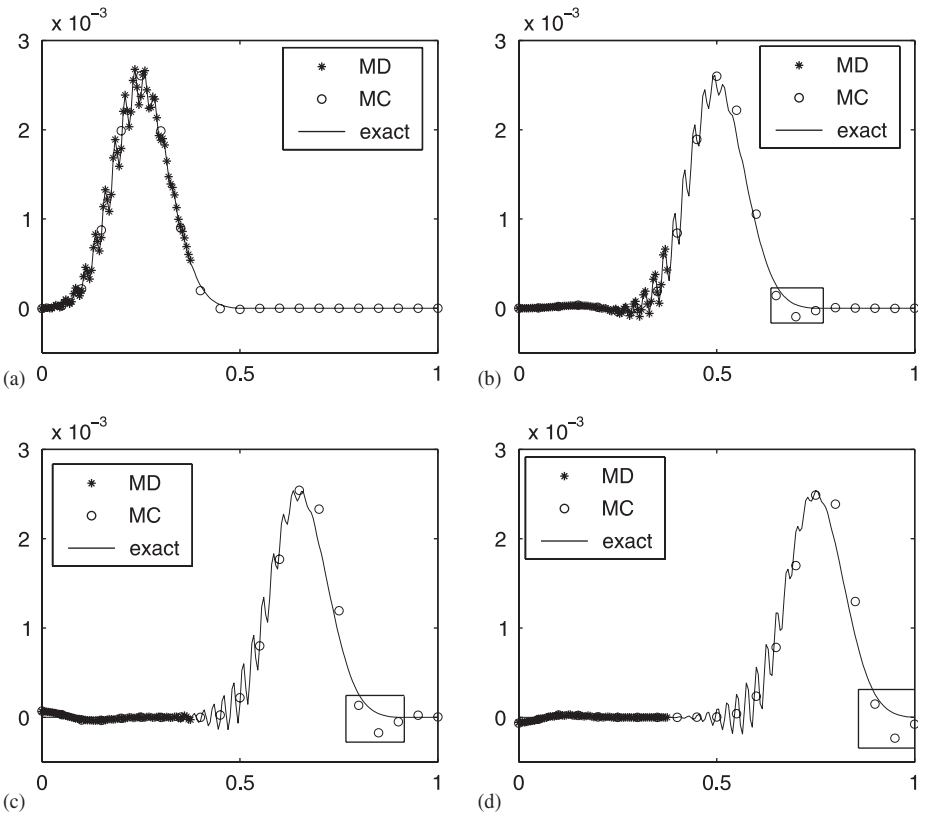

Figure 5. Harmonic lattice by BSM-LE (BSM with linear element): (a) $u(x, 50)$; (b) $u(x, 100)$; (c) $u(x, 130)$; and (d) $u(x, 150)$. Faster propagation speed is highlighted in the boxed region.

treatment. To find the error source, we make use of linearity, and compute separately the evolution with smooth initial data (mean part) and that with purely fluctuating initial data. From Figure 8(a), we observe that the residual in Ω_D is mainly due to smooth initial data. This is interpreted in the following way. Because the projection procedure maintains a continuous energy interchange between fine fluctuation and mean motion, u' becomes non-zero during the evolution, even if it is zero at a previous instant. The terms neglected in (49) and (50) cause matching error at the interface. The long wavelength reflection forms by the energy interchange mechanism. When we keep a longer time history, the fine fluctuations are suppressed, but this does not stop energy input from a coarse grid solution. As a result, global reflections remain at the same level. See Figure 8(b).

3.2. Anharmonic lattice

3.2.1. Physical setting and schemes. For an anharmonic lattice, we assume a potential function as

$$U(u) = U_1(u) + U_2(U) = \frac{1}{2}\sum_n (u_{n+1} - u_n)^2 + \frac{K}{4}\sum_n (u_{n+1} - u_n)^4 \tag{56}$$

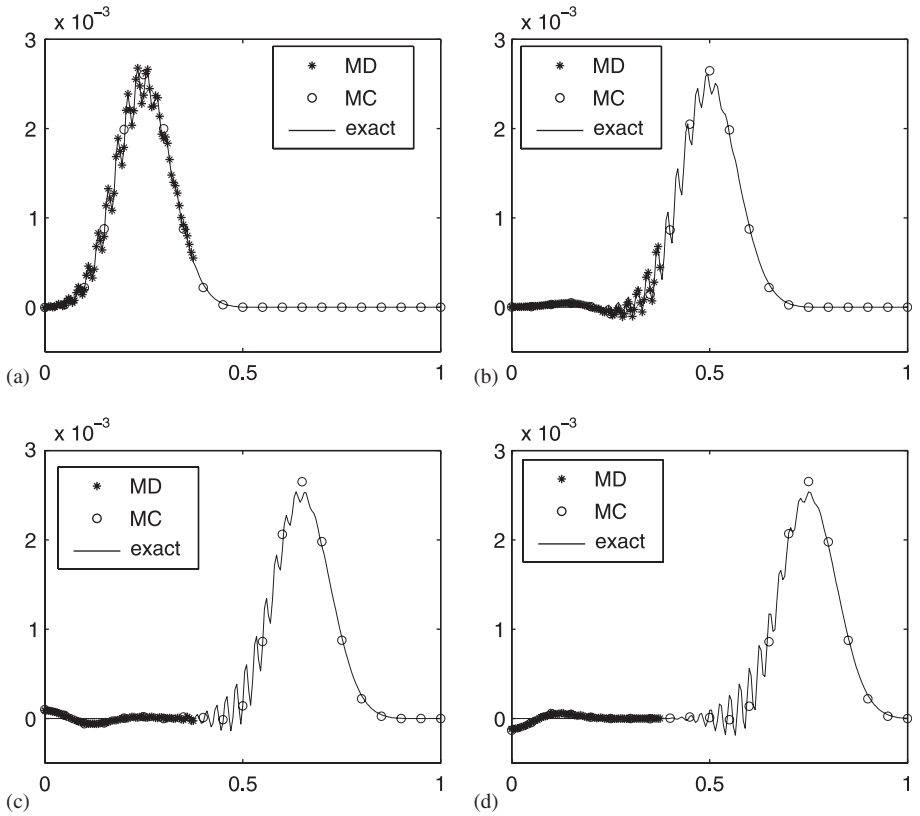

Figure 6. Harmonic lattice by BSM-MLE (BSM with modified linear element) scheme: (a) $u(x, 50)$; (b) $u(x, 100)$; (c) $u(x, 130)$; and (d) $u(x, 150)$.

Accordingly, the Newton equation is

$$\ddot{u}_n = u_{n-1} - 2u_n + u_{n+1} + K[(u_{n+1} - u_n)^3 - (u_n - u_{n-1})^3] \tag{57}$$

Though the mean displacement changes the time history kernel, we neglect this effect to reduce computing load. A harmonic lattice time history kernel is used.

For the coarse grid equations, we compute the internal force due to the non-linear potential, and obtain a concrete form of (6) as

$$(M\ddot{d})_I = \frac{1}{p}(u_{(I-1)p} - 2u_{Ip} + u_{(I+1)p}) + \frac{K}{p}\sum_{k=0}^{p-1}\left[(u_{Ip+k+1} - u_{Ip+k})^3 - (u_{(I-1)p+k+1} - u_{(I-1)p+k})^3\right] \tag{58}$$

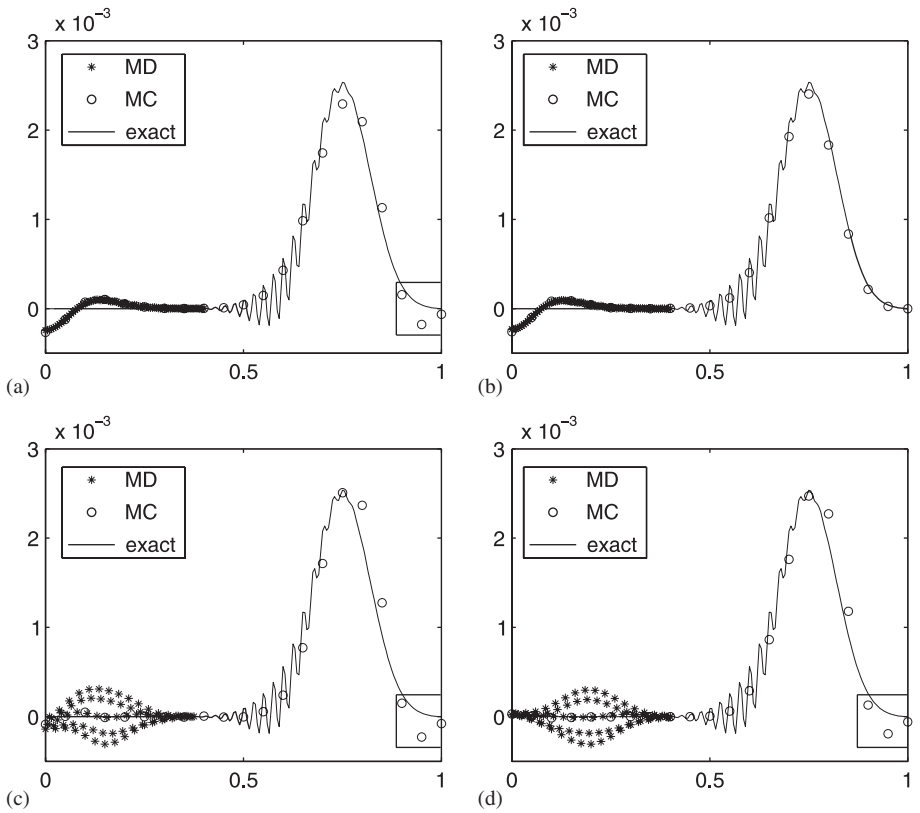

Figure 7. Harmonic lattice $u(x, 150)$: (a) the BSM-LE (BSM with linear element) scheme with enlarged Ω_D; (b) the BSM-MLE (BSM with modified linear element) scheme with enlarged Ω_D; (c) the BSM-LE (BSM with linear element) scheme without time history kernel technique; and (d) the BSM-LE (BSM with linear element) scheme with enlarged Ω_D, no time history kernel technique. Faster propagation speed is highlighted in the boxed regions for the results by the BSM-LE (BSM with linear element) scheme.

Dropping the fine fluctuations, we get an LE scheme (30)

$$(M\ddot{d})_I = \frac{1}{p}(d_{I-1} - 2d_I + d_{I+1}) + \frac{K}{p^3}[(d_{I+1} - d_I)^3 - (d_I - d_{I-1})^3] \tag{59}$$

Alternatively, we may derive an MLE scheme in a similar way as for the harmonic lattice. Denoting a vector V same as in the harmonic lattice, and a vector Z composed of the non-linear terms $\frac{K}{p^3}[(d_{I+1} - d_I)^3 - (d_I - d_{I-1})^3]$, we take twice time derivative of (58) as follows:

$$M\frac{\mathrm{d}^4}{\mathrm{d}t^4}d = \frac{D}{p}\ddot{V} + \ddot{Z} \approx \frac{D^2}{p^3}d + \left(\frac{\mathrm{d}^2}{\mathrm{d}t^2} + \frac{D}{p^2}\right)Z \tag{60}$$

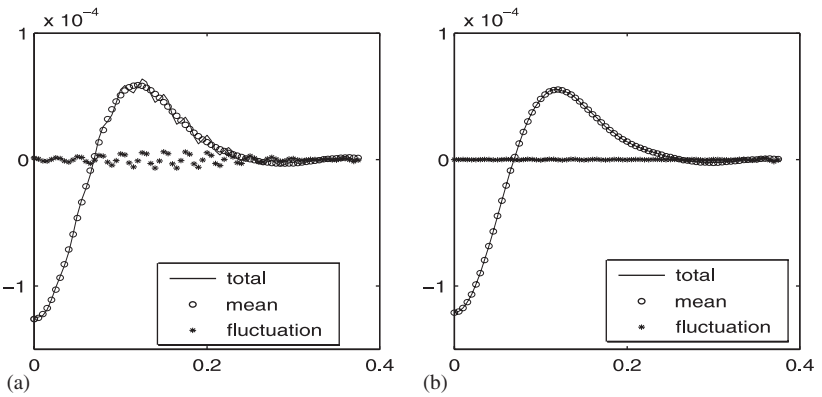

Figure 8. Error source in harmonic lattice by BSM-MLE (BSM with modified linear element) scheme, time history cut-off: (a) $T=5$; and (b) $T=50$.

Making operator decomposition and a further approximation, we have

$$\left(\sqrt{M}\frac{\mathrm{d}^2}{\mathrm{d}t^2}-\frac{D}{\sqrt{p^3}}\right)d=\left(\sqrt{M}\frac{\mathrm{d}^2}{\mathrm{d}t^2}-\frac{D}{\sqrt{p^3}}\right)^{-1}\left(\frac{\mathrm{d}^2}{\mathrm{d}t^2}+\frac{D}{p^2}\right)Z\approx\frac{Z}{\sqrt{M}} \tag{61}$$

3.2.2. Numerical results. For the anharmonic lattice, we take numerical parameters and initial data the same as for the harmonic lattice, and non-linear coefficient $K=10/h_a^2$ with $h_a=0.005$. Solutions $u(x,t)$ at time $t=50, 100, 130, 150$ are displayed in Figure 9 for the BSM-LE scheme. At $t=50$, the primary wave starts to go across the interface, whereas fluctuations do not. The solutions are not discernable from the exact solution. At $t=100$, fluctuations go across the interface, and minor reflection is observed. We remark that at this moment, the assumption of linear dependence of internal force on u'_C does not hold. Theoretically multiscale methods may fail. However, we still obtain a reasonable resolution. At $t=150$, the wave has left Ω_D, leaving behind a fairly small amount of energy. On the other hand, if we use the BSM-MLE scheme instead, the coarse grid solution in Ω_C has a better resolution, as shown in Figure 10. However, this does not reduce reflection in Ω_D.

3.3. Lennard–Jones potential

A Lennard–Jones potential is widely used in studies at the microscopic scale. For a displacement vector $u=(u_1,\ldots,u_N)^{\mathrm{T}}$, the potential function is

$$U(u)=4\varepsilon\sum_n\left[\left(\frac{\sigma}{r_0+u_{n+1}-u_n}\right)^{12}-\left(\frac{\sigma}{r_0+u_{n+1}-u_n}\right)^{6}\right] \tag{62}$$

with r_0 the atom distance at rest, σ the collision diameter and ε the bonding/dislocation energy. In our numerical tests, we take the rescaled values as $\sigma=\varepsilon=1$, and correspondingly $r_0=2^{1/6}$.

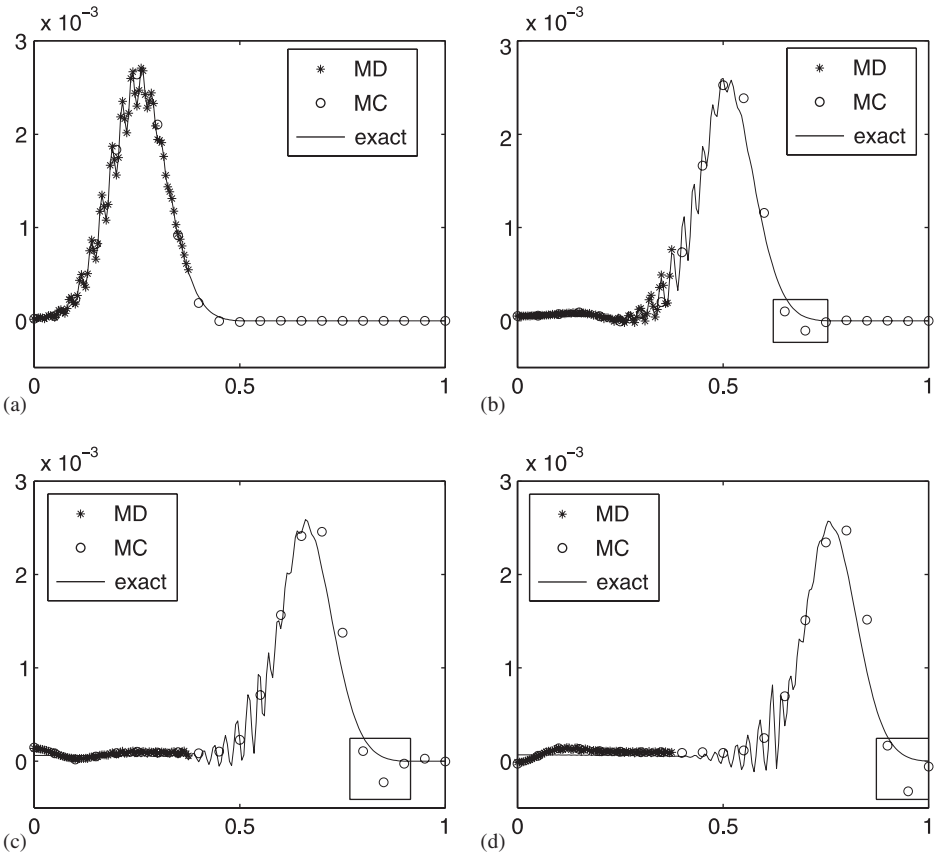

Figure 9. Anharmonic lattice with $K = 10/h_a^2$ by the BSM-LE (BSM with linear element) scheme: (a) $u(x, 50)$; (b) $u(x, 100)$; (c) $u(x, 130)$; and (d) $u(x, 150)$. Faster propagation speed is highlighted in the boxed regions.

The governing equation for the displacement u_n is

$$\begin{aligned}\ddot{u}_n = &-48[(r_0 + u_{n+1} - u_n)^{-13} - (r_0 + u_n - u_{n-1})^{-13}] \\ &+24[(r_0 + u_{n+1} - u_n)^{-7} - (r_0 + u_n - u_{n-1})^{-7}]\end{aligned} \tag{63}$$

The LE scheme is reduced to

$$\begin{aligned}(M\ddot{d})_I = &-48\left[\left(r_0 + \frac{u_{n+1} - u_n}{p}\right)^{-13} - \left(r_0 + \frac{u_n - u_{n-1}}{p}\right)^{-13}\right] \\ &+24\left[\left(r_0 + \frac{u_{n+1} - u_n}{p}\right)^{-7} - \left(r_0 + \frac{u_n - u_{n-1}}{p}\right)^{-7}\right]\end{aligned} \tag{64}$$

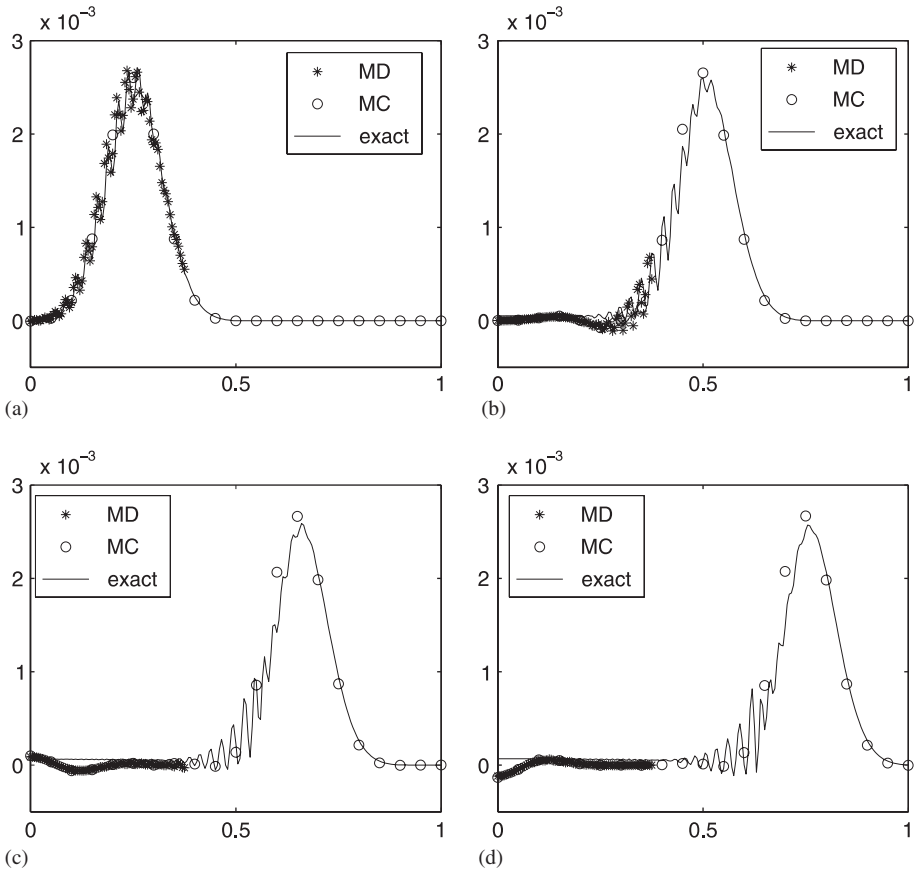

Figure 10. Anharmonic lattice with $K = 10/h_a^2$ by BSM-MLE (BSM with modified linear element) scheme: (a) $u(x, 50)$; (b) $u(x, 100)$; (c) $u(x, 130)$; and (d) $u(x, 150)$.

The curvature of U at r_0 is $k = 624r_0^{-14} - 168r_0^{-8} = 72/\sqrt[3]{2}$. The time history kernel function is

$$\theta(t) = 2J_2(2\sqrt{k}t)/t \tag{65}$$

In our numerical experiment, we take 41 coarse grid points in $\Omega = [-200r_0, 200r_0]$ ($p = 10$), and $\triangle t = 0.01$. The MD region is $\Omega_D = [-55r_0, 55r_0]$ with 111 atoms, computed with $\triangle\tau = 0.001$. The initial data is

$$u(x) = \begin{cases} 0.015\dfrac{\mathrm{e}^{-(x/20)^2} - \mathrm{e}^{25}}{1 - \mathrm{e}^{25}}(1 + 0.2\cos(2\pi x/80)) & |x| < 100 \\ 0 & \text{elsewhere} \end{cases} \tag{66}$$

Numerical solutions at $t = 6, 9, 12, 20$ are displayed in Figure 11. Basic features are similar to the anharmonic lattice. Agreement with the exact solutions is quite good up to about $t = 9$, when

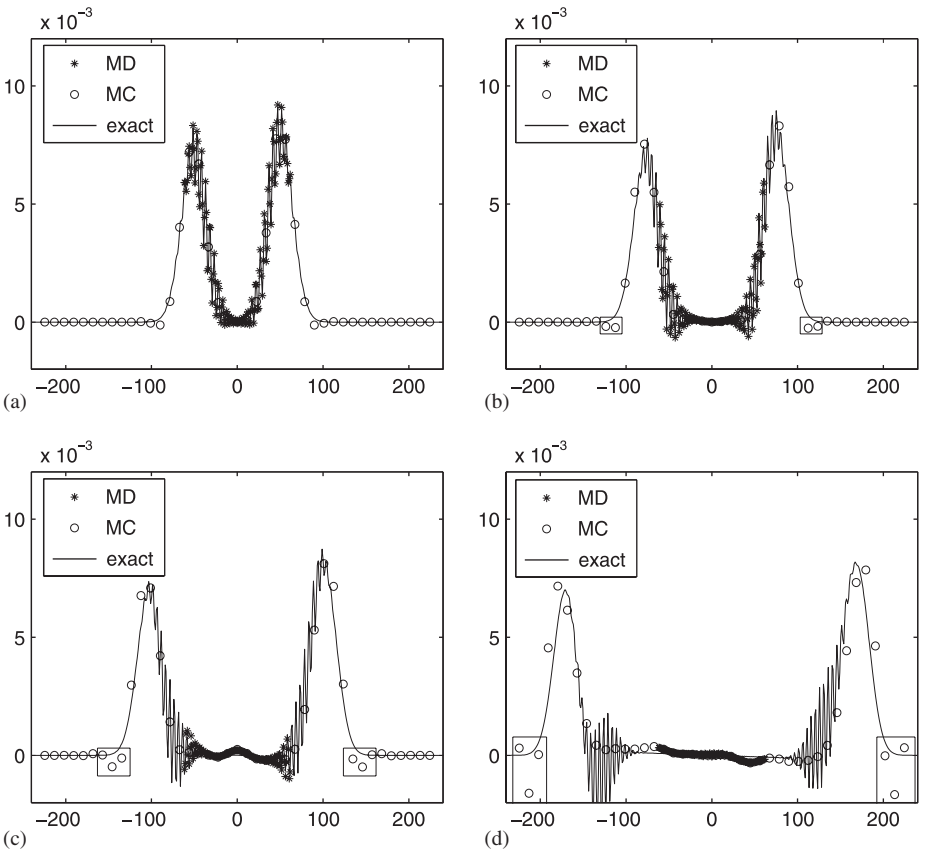

Figure 11. Lattice with Lennard–Jones potential, by the BSM-LE (BSM with linear element) scheme: (a) $u(x, 6)$; (b) $u(x, 9)$; (c) $u(x, 12)$; and (d) $u(x, 20)$. Faster propagation speed is highlighted in the boxed regions.

the fluctuation partly goes across the interface. Though the condition required for validating the multiscale methods fails, our numerical scheme still performs very well in a later stage. In particular, reflections in Ω_D are fairly small.

4. DISCUSSIONS

In this paper, we have formulated the BSM for simulating complex systems. This is the first rigorous and systematic derivation for BSM. Through the study, we have clearly identified the conditions for using the method, and analysed the error sources.

We summarize the conditions for applying BSM as follows:

- Active non-linear fluctuation occurs only in a localized sub-domain Ω_D.
- Atomistic forces depend on u'_C nearly in a linear way.
- The linear dependence on u'_C is well characterized by a time-independent matrix K.

These conditions actually amount to a linear approximation for the fine fluctuations across the interface. A special case satisfying the second condition is when $\|u'_C\| \ll 1$ under certain suitable norm. The third condition may be relaxed to a slowly time varying K, for which we may update time history kernel Φ_G after a suitable time. We remark that the whole algorithm still remains non-linear, because of a non-linear coarse grid scheme and non-linear MD computations.

The BSM adopts the linear element approximation and defines the coarse scale displacement d. In Ω_C, the mean displacement is represented by interpolating d. Since d has a much smaller degree of freedom, the computing load and memory requirement are considerably reduced. Furthermore, in MD region, a full atomistic computation is performed to resolve the active dynamics. An approximated time history treatment is applied to the fine fluctuations, in order to reduce the reflections due to the abrupt termination of the MD region. Typically the fine fluctuation part only represents a small portion of the total energy, and the treatment is quite effective. The computation of time history convolution makes up the main additional computing load and memory requirement. We remark that there are fast convolution techniques [32].

In the BSM algorithm, we have made the following approximations:

- In the coarse grid equation for d and the reassignment of it, the contribution of the fine fluctuations is not fully resolved.
- Across the interfaces between Ω_C and Ω_D, a linear constant K is taken into account for the effect of u'_C.
- In the interfacial conditions, a leading order approximation is made with respect to the coarsening ratio, to alleviate computing load for evaluating convolutions.
- The convolution is performed with a truncated time history.

From our clear derivations and numerical experiments, we identify the error source in BSM as follows:

- Approximation in the coarse grid equations with the LE scheme. We may improve this by the MLE scheme.
- Simplification in the interfacial conditions. This causes an energy interchange between the fine fluctuation and mean displacement across the interfaces. Minor reflections appear in Ω_D, with a dependency to the choice of Ω_D.

In the current framework, it is not easy to handle the second error source. If we adopt the precise interfacial condition, the numerical cost in evaluating all convolutions is expensive. Furthermore, though the error in this simplification formally decreases as the coarsening ratio increases, we should be cautious in increasing the ratio for maintaining accuracy in coarse grid. If the ratio is too large, we may fail to resolve the waves associated with the macroscopic solution. We further remark that in a pseudo-spectral multiscale method [26], a balanced accuracy and efficiency may be achieved for the coarse and fine scales, and the interfaces. Moreover, a matching differential operator approach has been proposed to design accurate and efficient coarse grid equations for multi-dimensional linear and non-linear lattice systems.

In addition to deriving a clear and consistent formulation, we also present a numerical algorithm that is slightly different from its original version in Reference [1]. In particular, with the exact evolution Equations (11) and (12), we do not need to introduce a supplementary variable q for computing the fine fluctuations in the MD region. Though these differences do not strongly affect the accuracy, they help in making the BSM algorithm clearer and the

implementation easier. Some further features of this formulation are as follows:

- We use an overlapping region and consistently adopt the projection operator to pass information between the coarse and fine scales. We therefore obtain a clear algorithm for coarse scale dynamics, and avoid empirical descriptions such as a mixed Hamiltonian.
- With the projection operator, we derive the precise equation for u', and the multiscale interfacial condition that is exact for linear lattices.
- We develop more accurate coarse grid schemes (MLE), which better resolve the dynamics in Ω_C.

Among many challenging issues in further developing BSM, we note some topics under consideration. First, from the perspective of numerical methods, a rigorous study of convergence and accuracy may help further improvement. Secondly, we currently use a fixed MD region and a time-independent K, describing the linear dependence on fine fluctuations in Ω_C. An adaptive MD region and time-dependent K may further enhance the capability of these methods. Moreover, if we discard the linear dependency, more sophisticated homogenization techniques are required to decouple the coarse and fine scales.

APPENDIX A: VIRTUAL ATOM CLUSTER METHOD

While many inter-atomic components may appear, we demonstrate the idea with pairwise potential. It involves atom distances (within cut-off radius) in the form of $U(u) = \sum_{\alpha\neq\beta} \Psi(r_{\alpha\beta})$, with $r_{\alpha\beta} = r^0_{\alpha\beta} + u_\alpha - u_\beta$ and $r^0_{\alpha\beta}$ the rest distance.

In Ω_C, one neglects fine fluctuations in u_α and u_β to get

$$r_{\alpha\beta} \approx \bar{r}_{\alpha\beta} = r^0_{\alpha\beta} + \sum_J (N_{\alpha J} - N_{\beta J}) d_J \tag{A1}$$

As a result, the internal force may be approximated by a function of $\bar{r}$ and hence of d as $\sum_{\alpha\neq\beta} \frac{\partial\Psi}{\partial r_{\alpha\beta}}(\bar{r}_{\alpha\beta})(N_{\alpha J} - N_{\beta J})$. We end up with a coarse grid equation

$$(M\ddot{d})_J \approx \sum_{\alpha\neq\beta} \frac{\partial\Psi}{\partial r_{\alpha\beta}}(r_{\alpha\beta})(N_{\alpha J} - N_{\beta J}) + \sum_\alpha N_{\alpha J} f_{\text{ext},\alpha} \tag{A2}$$

where $r_{\alpha\beta}$ is approximated by $\bar{r}_{\alpha\beta}$ for atoms outside of Ω_D.

APPENDIX B: DISPERSION RELATIONS

For a given wave number ω, we assume that the solution to the harmonic lattice Equation (33) takes the form of $u_n(t) = e^{i(\lambda t - \omega n)}$. Substituting it into the equation, we obtain

$$-\lambda^2 e^{i(\lambda t-\omega n)} = e^{i(\lambda t-\omega(n-1))} - 2e^{i(\lambda t-\omega n)} + e^{i(\lambda t-\omega(n+1))} \tag{B1}$$

This gives $\lambda = 2\sin(\omega/2)$.

Similarly, we assume that the numerical solution to the LE scheme (38) takes the form of $d_J(t) = e^{i(\lambda t - \omega J p)}$. With the explicit expression (36) of M, the scheme reads

$$-\lambda_{\mathrm{LE}}^2(\beta e^{i(\lambda t-\omega(J-1)p)} + \alpha e^{i(\lambda t-\omega J p)} + \beta e^{i(\lambda t-\omega(J+1)p)}) = \frac{1}{p}(e^{i(\lambda t-\omega(J-1)p)} - 2e^{i(\lambda t-\omega J p)} + e^{i(\lambda t-\omega(J+1)p)}) \tag{B2}$$

After some manipulations, we obtain

$$\lambda_{\mathrm{LE}} = \frac{2\sin(\omega p/2)}{\sqrt{p^2 - 2(p^2-1)\sin^2(\omega p/2)/3}} \tag{B3}$$

For the MLE scheme (45), we obtain in a similar way that

$$\lambda_{\mathrm{MLE}} = \frac{2\sin(\omega p/2)}{\sqrt[4]{p^4 - 2p^2(p^2-1)\sin^2(\omega p/2)/3}} \tag{B4}$$

ACKNOWLEDGEMENTS

We would like to thank the anonymous referees, Dr Eduard Karpov, Dr Harold Park, Mr Justin Mach and Mr Wuan Luo for stimulating discussions. We would also like to thank the NSF Summer Institute of Nano Mechanics and Materials, and the Army Research Office (ARO) for their support of this research.

REFERENCES

1. Wagner GJ, Liu WK. Coupling of atomistic and continuum simulations using a bridging scale decomposition. *Journal of Computational Physics* 2003; **190**:249–274.
2. Engquist B, Majda A. Radiation boundary conditions for acoustic and elastic calculations. *Communication on Pure Applied Mathematics and Analysis* 1979; **32**:313–357.
3. Givoli D, Keller JB. Non-reflecting boundary conditions for elastic waves. *Wave Motion* 1990; **12**:261–279.
4. Grote MJ, Keller JB. Nonreflecting boundary conditions for time-dependent scattering. *Journal of Computational Physics* 1996; **127**:52–65.
5. Higdon RL. Radiation boundary conditions for dispersive waves. *SIAM Journal on Numerical Analysis* 1994; **31**:64–100.
6. Kohlhoff S, Gumbsch P, Fischmeister HF. Crack propagation in BCC crystals studied with a combined finite element and atomistic model. *Philosophical Magazine A—Physics of Condensed Matter Structure Defects and Mechanical Properties* 1991; **64**:851–878.
7. Abraham FF, Broughton JQ, Bernstein N, Kaxiras E. Spanning the length scales in dynamic simulation. *Computers in Physics* 1998; **12**:538–546.
8. Broughton JQ, Abraham FF, Bernstein N, Kaxiras E. Concurrent coupling of length scales: methodology and application. *Physical Review B* 1999; **60**:2391–2403.
9. Rudd RE, Broughton JQ. Concurrent coupling of length scales in solid state systems. *Physica Status Solidi* 2000; **217**:251–291.
10. Xiao SP, Belytschko T. A bridging domain method for coupling continua with molecular dynamics. *Computer Methods in Applied Mechanics and Engineering* 2004; **193**:1645–1669.
11. Basu U, Chopra A. Perfectly matched layers for time-harmonic elastodynamics of unbounded domains: theory and finite-element implementation. *Computer Methods in Applied Mechanics and Engineering* 2003; **192**:1337–1375.
12. To AC, Li S. Perfectly matched multiscale simulations, preprint.

13. Knap J, Ortiz M. Effect of indenter-radius size on Au(001) nanoindentation. *Physical Review Letters* 2003; **90**:226102.
14. Tadmor EB, Miller R, Phillips R, Ortiz M, Mater J. Nano-indentation and incipient plasticity. *Journal of Materials Research* 1999; **14**:2233–2250.
15. Tadmor EB, Ortiz M, Phillips R. Quasicontinuum analysis of defects in solids. *Philosophical Magazine A—Physics of Condensed Matter Structure Defects and Mechanical Properties* 1996; **73**:1529–1563.
16. Shilkrot LE, Curtin WA, Miller RE. Coupled atomistic and discrete dislocation plasticity. *Physical Review Letters* 2002; **89**:025501.
17. Shilkrot LE, Miller RE, Curtin WA. Multiscale plasticity modeling: coupled atomistics and discrete dislocation mechanics. *Journal of the Mechanics and Physics of Solids* 2004; **52**:755–787.
18. Adelman SA, Doll JD. Generalized Langevin equation approach for atom/solid-surface scattering: collinear atom/harmonic chain model. *Journal of Chemical Physics* 1974; **61**:4242–4245.
19. Cai W, de Koning M, Bulatov VV, Yip S. Minimizing boundary reflections in coupled-domain simulations. *Physical Review Letters* 2000; **85**:3213–3216.
20. Karpov EG, Park HS, Liu WK, Dorofeev DL. On the modelling of chaotic thermal motion in solids, preprint.
21. Liu WK, Karpov EG, Zhang S, Park HS. An introduction to computational nanomechanics and materials. *Computer Methods in Applied Mechanics and Engineering* 2004; **193**:1529–1578.
22. Park HS, Karpov EG, Liu WK, Klein PA. The bridging scale for two-dimensional atomistic/continuum coupling. *Philosophical Magazine* 2005; **85**:79–113.
23. E W, Ming P, Zhang P. Analysis of the heterogeneous multiscale method. *Journal of the American Mathematical Society* 2004; **18**:121–156.
24. Oden JT, Prudhomme S, Romkes A, Bauman P. Multi-scale modeling of physical phenomena: adaptive control of models, preprint.
25. Qian D, Wagner GJ, Liu WK. A multiscale projection method for the analysis of carbon nanotubes. *Computer Methods in Applied Mechanics and Engineering* 2004; **193**:1603–1632.
26. Tang S, Hou TY, Liu WK. A pseudo-spectral multiscale method: interfacial conditions and coarse grid equations. *Journal of Computational Physics*, in press.
27. Karpov EG, Wagner GJ, Liu WK. A Green's function approach to deriving non-reflecting boundary conditions in molecular dynamics simulations. *International Journal for Numerical Methods in Engineering* 2005; **62**:1250–1262.
28. Wagner GJ, Karpov EG, Liu WK. Molecular dynamics boundary conditions for regular crystal lattices. *Computer Methods in Applied Mechanics and Engineering* 2004; **193**:1579–1601.
29. O'Connell ST, Thompson PA. Molecular dynamics-continuum hybrid computations: a tool for studying complex fluid flows. *Physical Review E* 1995; **52**:R5792–R5795.
30. Nie XB, Chen SY, E W, Robbins MO. A continuum and molecular dynamics hybrid method for micro- and nano-fluid flow. *Journal of Fluid Mechanics* 2004; **500**:55–64.
31. E W, Huang Z. A dynamic atomistic-continuum method for simulation of crystalline materials. *Journal of Computational Physics* 2002; **182**:234–261.
32. Lubich C, Schaedle A. Fast convolution for nonrefelecting boundary conditions. *SIAM Journal on Scientific Computing* 2002; **24**:161–182.

